Letters

Misalignment-Tolerant Dual-Transmitter Electric Vehicle Wireless Charging System With Reconfigurable Topologies

Yiming Zhang, *Senior Member, IEEE*, Wenbin Pan, Hui Wang, Zhiwei Shen, Yuanchao Wu, Jiqing Dong, and Xingkui Mao

***Abstract*—Wireless charging for electric vehicles (EVs) enjoys many benefits, such as convenience, safety, and automation. One of the major issues concerning EV wireless charging is misalignment tolerance along the door-to-door direction of the EV. This letter proposes a misalignment-tolerant dual-transmitter EV wireless charging system with a reconfigurable topology. At central positions, the system can be reconfigured to the S-S (series-series) topology where the two transmitting coils are connected in series to feed the load. At boundary positions, the two transmitting coils form the LCCC-S (inductor-capacitor-capacitor-capacitor-series) topology to enhance power transfer capability and tolerate weak couplings. In this way, not only the output power can be smoothed with door-to-door misalignment, but also wireless charging is guaranteed at weak couplings. Experimental results reveal that within the cover area of the transmitting coils, high-efficiency stable output can be achieved.**

***Index Terms*—Dual transmitter, misalignment tolerance, reconfigurable, wireless charging, wireless power transfer (WPT).**

I. Introduction

TO DEAL with global warming and extreme weather conditions, developing and using renewable energy is a must. The carbon emission in the transportation field accounts for a large proportion of the total carbon emission. Transportation electrification can greatly reduce carbon emission. Electric vehicles (EVs) play a crucial role in transportation electrification and have developed rapidly in the recent decade [1].

One of the obstacles facing EVs is the charging issue. With conventional conductive charging, users need to touch the dirty and heavy charger, which is inconvenient. Also, hazards can happen in rainy or snowy weather. Wireless power transfer (WPT) is an emerging technology that has the advantages of automation, safety, convenience, and feasibility to various conditions. EV wireless charging has gained increasing attention in recent years due to these advantages [2], [3].

Manuscript received January 25, 2022; revised March 2, 2022; accepted March 15, 2022. Date of publication March 22, 2022; date of current version April 28, 2022. This work was supported in part by the National Natural Science Foundation of China under Grant 52107183 and in part by the State Key Laboratory of Power System and Generation Equipment under Grant SKLD21KZ05. *(Corresponding author: Xingkui Mao.)*

The authors are with the School of Electrical Engineering and Automation, and also with Fujian Key Laboratory of New Energy Generation and Power Conversion, Fuzhou University, Fuzhou 350108, China (e-mail: zhangym07@gmail.com; 210120060@fzu.edu.cn; 210127144@fzu.edu.cn; 210127138@fzu.edu.cn; 210120068@fzu.edu.cn; dongjiqing@fzu.edu.cn; mxk782@fzu.edu.cn).

Color versions of one or more figures in this article are available at https://doi.org/10.1109/TPEL.2022.3160868.

Digital Object Identifier 10.1109/TPEL.2022.3160868

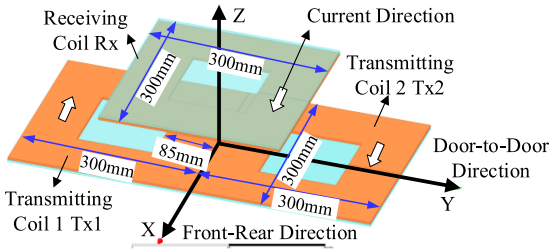

Fig. 1. Coil structure of dual-transmitter WPT system.

In EV wireless charging systems, misalignment between the transmitting and receiving coils can happen since drivers cannot always park the car in the exact position. There are two directions for misalignment: front-rear direction and door-to-door direction. Drivers can adjust the front-rear direction more easily than the door-to-door direction. Thus, the door-to-door misalignment is more crucial. The misalignment tolerance for the door-to-door direction should be enhanced.

Current solutions for misalignment tolerance include magnetic coupler design, compensation networks, power electronics converters, and the control. In magnetic coupler design, a smaller winding width was proved to enhance the capability for misalignment tolerance [4]. Bipolar coils [5] and solenoid coils [6] were optimized for misalignment tolerance. Antiparallel windings [7], [8] were adopted. In compensation networks, hybrid compensations [9]–[11], namely a combination of different compensations such as series and LCC (inductor-capacitor-capacitor) compensations, can improve misalignment tolerance. Power electronics converters and the control were also designed to achieve this target [12]–[14].

This letter proposes a misalignment-tolerant dual-transmitter EV wireless charging system based on reconfigurable topologies. S-S (series-series) and LCCC-S (inductor-capacitor-capacitor-capacitor-series) topologies can be switched. In this way, high-efficiency stable output power can be achieved with large misalignment.

II. Proposed Reconfigurable WPT System

A. Coil Structure

To increase the door-to-door misalignment tolerance, two square transmitting coils (Tx1 and Tx2) are placed side by side, and the receiving coil (Rx) is placed above the transmitting coils, as shown in Fig. 1. The charging distance is 100 mm.

With the defined current directions in Fig. 1, when Rx moves from the left edge of Tx1 to the right edge of Tx2, the coupling coefficients are depicted in Fig. 2, where k_{T12} is the coupling coefficient of Tx1 and Tx2, and k_{T1R} (k_{T2R}) is the coupling

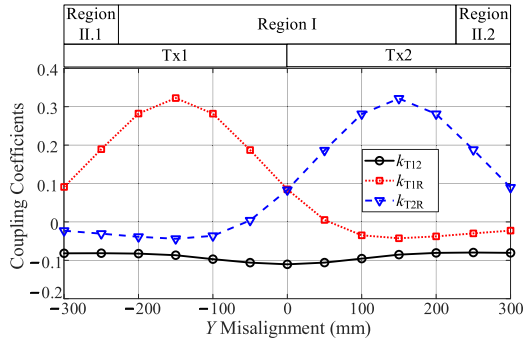

Fig. 2. Coupling coefficients varying with *Y* misalignment.

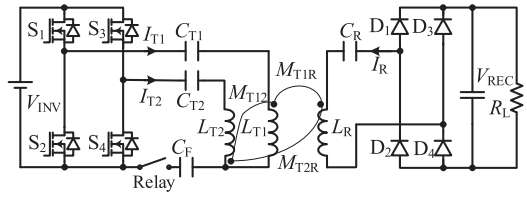

Fig. 3. Proposed WPT system with reconfigurable topologies.

coefficient of Tx1 (Tx2) and Rx. From Fig. 2, k_{T12} is relatively stable with misalignment. However, k_{T1R} and k_{T2R} change rapidly with misalignment and peak when fully aligned. Beyond a certain misalignment, k_{T1R} and k_{T2R} become negative, indicating that the dotted terminals have reversed their direction. The charging area is divided into three regions: Regions I, II.1, and II.2, as shown in Fig. 2.

B. System Topology

The S-S topology is the most popular topology with the advantages of independent compensation from loading and coupling conditions. However, with a constant-voltage supply, its output power increases with the decreasing coupling coefficient. Thus, it is not suitable when large misalignment occurs. In contrast, with primary-side LCC compensation under a constant-voltage source, the output power decreases with the decreasing coupling coefficient. Thus, the primary-side LCC compensation is suitable when larger misalignment occurs.

This letter proposes a reconfigurable WPT system that can switch between the S-S and LCCC-S topologies, as shown in Fig. 3. S_1-S_4 are the inverter switches and D_1-D_4 are the rectifier diode. V_{INV} (V_{REC}) is the inverter (rectifier) dc voltage. L_{T1}, L_{T2}, and L_R are the inductances of Tx1, Tx2, and L_R, respectively, with I_{T1}, I_{T2}, and I_R as the respective coil current. C_{T1}, C_{T2}, C_F, and C_R are the compensating capacitances. M_{T1R}, M_{T2R}, and M_{T12} are mutual inductances. R_L is the load resistance. A relay is added between C_F and the negative dc bus for reconfiguring purposes.

The system works at the resonant angular frequency ω

$$\omega = \frac{1}{\sqrt{L_R C_R}} = \frac{1}{\sqrt{L_{T1}\frac{C_F C_{T1}}{C_F + C_{T1}}}} = \frac{1}{\sqrt{L_{T2}\frac{C_F C_{T2}}{C_F + C_{T2}}}}. \quad (1)$$

C_{T1}, L_{T1}, and C_F constitute a resonant loop. C_{T2}, L_{T2}, and C_F form the second resonant loop. L_R and C_R form the third.

III. Working Modes and Modeling

A. Mode I: S-S Topology

At Region I as shown in Fig. 2, Rx couples with Tx1 and Tx2. In this condition, Tx1 and Tx2 are connected in series, forming an S-S topology with a dual-transmitter structure, as shown in Fig. 4.

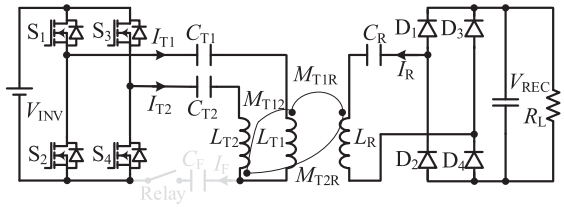

Fig. 4. Mode I: Opening relay to form S-S topology with a dual-transmitter structure.

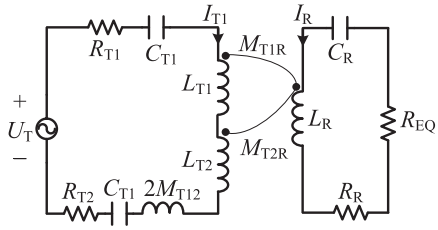

Fig. 5. Equivalent circuit of S-S topology in Mode I.

The relay is open at this mode. The equivalent circuit of Mode I is given in Fig. 5. Tx1 and Tx2 are decoupled by using one equivalent series inductance $2M_{T12}$. Please note that M_{T12} is negative. R_{T1}, R_{T2}, and R_R are the equivalent resistance of Tx1, Tx2, and Rx, respectively. U_T is the fundamental component of the inverter ac voltage. R_{EQ} is the equivalent ac load resistance.

Employing first harmonic approximation yields

$$U_T = \frac{2\sqrt{2}}{\pi} V_{INV}, R_{EQ} = \frac{8}{\pi^2} R_L. \quad (2)$$

Based on Kirchhoff's Voltage Law (KVL) and ignoring R_{T1}, R_{T2}, and R_R, we have

$$\begin{cases} \boldsymbol{U_T} = \begin{pmatrix} \mathrm{j}\omega L_{T1} + \frac{1}{\mathrm{j}\omega C_{T1}} + \mathrm{j}\omega L_{T2} \\ + \frac{1}{\mathrm{j}\omega C_{T2}} + \mathrm{j}2\omega M_{T12} \end{pmatrix} \boldsymbol{I_{T1}} \\ + \begin{pmatrix} \mathrm{j}\omega M_{T1R} \\ + \mathrm{j}\omega M_{T2R} \end{pmatrix} \boldsymbol{I_R} \\ (\mathrm{j}\omega M_{T1R} + \mathrm{j}\omega M_{T2R})\, \boldsymbol{I_{T1}} \\ + \left(\mathrm{j}\omega L_R + \frac{1}{\mathrm{j}\omega C_R} + R_{EQ}\right) \boldsymbol{I_R} = 0 \end{cases} \quad (3)$$

Combining (1) and (3), the input impedance Z_{IN} is

$$Z_{IN} = \frac{\omega^2 (M_{T1R} + M_{T2R})^2}{R_{EQ}} + \mathrm{j}2X_T \quad (4)$$

in which X_T is the reactance defined as follows:

$$X_T = \frac{1}{\omega C_F} + \omega M_{T12} = \frac{1}{\omega C_F} - \omega |M_{T12}| \quad (5)$$

Please note that M_{T12} is negative. By designing X_T larger than 0, Z_{IN} can be inductive so that zero voltage switching (ZVS) can be realized.

The output voltage, output power, and coil-to-coil efficiency can be calculated as follows:

$$V_{REC} = \frac{V_{INV}}{\sqrt{\frac{\pi^4}{64}\frac{\omega^2 (M_{T1R}+M_{T2R})^2}{R_L^2} + \frac{4X_T^2}{\omega^2 (M_{T1R}+M_{T2R})^2}}}. \quad (6)$$

$$P_{OUT} = \frac{V_{INV}^2}{\frac{\pi^4}{64}\frac{\omega^2 (M_{T1R}+M_{T2R})^2}{R_L} + \frac{4R_L X_T^2}{\omega^2 (M_{T1R}+M_{T2R})^2}}. \quad (7)$$

$$\eta = \frac{P_{out}}{P_{out} + (R_{T1} + R_{T2})\, I_{T1}^2 + R_R I_R^2} \quad (8)$$

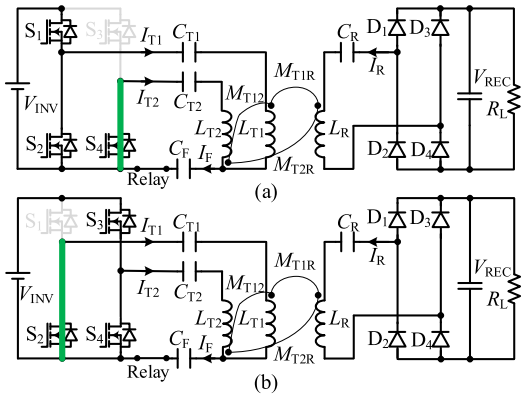

Fig. 6. Mode II: Closing relay to form LCCC-S topology. (a) Tx2 as power transmission coil. (b) Tx1 as power transmission coil.

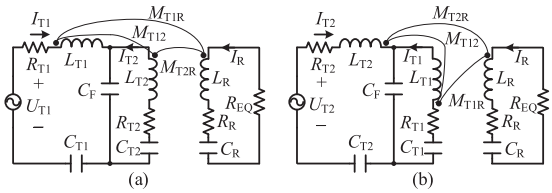

Fig. 7. Equivalent circuits of LCCC-S topology in Mode II. (a) Tx2 as power transmission coil. (b) Tx1 as power transmission coil.

From (6) we can see that the two terms under the square root sign have opposite changing directions with (M_{T1R}+M_{T2R}): one is proportional, and the other is in reverse proportion. Thus, by designing the system around the peak point, which is the extremum value, the variation of V_{REC} with (M_{T1R}+M_{T2R}) can be smoothed. The condition to achieve the peak point is

$$R_{\mathrm{L}} = \frac{\pi^2}{16}\frac{\omega^2(M_{\mathrm{T1R}} + M_{\mathrm{T2R}})^2}{X_{\mathrm{T}}} \tag{9}$$

B. Mode II: LCCC-S Topology

At Region II.2 when Rx is above Tx2, Tx2 acts as the power transmission coil, and Tx1 acts as the compensating inductor. In this condition, S_3 is constantly on and S_4 is constantly off, forming the LCCC compensation, as shown in Fig. 6(a). At Region II.2 when Rx is above Tx1, Tx1 acts as the power transmission coil and Tx2 acts as the compensating inductor. In this condition, S_1 is constantly on and S_2 is constantly off, also forming the LCCC compensation, as shown in Fig. 6(b). The equivalent circuits of Fig. 6 are depicted in Fig. 7. U_{T1} (U_{T2}) is the output voltage of the phases S_1 and S_2 (S_3 and S_4). They can be expressed as follows:

$$U_{\mathrm{T1}} = U_{\mathrm{T2}} = \frac{\sqrt{2}}{\pi}V_{\mathrm{INV}}. \tag{10}$$

Take Fig. 7(a) as an example. Based on KVL and ignoring R_{F}, R_{T}, and R_{R}, we have

$$\begin{cases} \boldsymbol{U_{\mathrm{T1}}} = \left(\mathrm{j}\omega L_{\mathrm{T1}} + \frac{1}{\mathrm{j}\omega C_{\mathrm{T1}}} + \frac{1}{\mathrm{j}\omega C_{\mathrm{F}}}\right)\boldsymbol{I_{\mathrm{T1}}} \\ +\mathrm{j}\omega M_{\mathrm{T1R}}\boldsymbol{I_{\mathrm{R}}} + \left(\frac{1}{\mathrm{j}\omega C_{\mathrm{F}}} - \mathrm{j}\omega M_{\mathrm{T12}}\right)\boldsymbol{I_{\mathrm{T2}}} \\ 0 = \left(\mathrm{j}\omega L_{\mathrm{T2}} + \frac{1}{\mathrm{j}\omega C_{\mathrm{T2}}} + \frac{1}{\mathrm{j}\omega C_{\mathrm{F}}}\right)\boldsymbol{I_{\mathrm{T2}}} \\ -\mathrm{j}\omega M_{\mathrm{T2R}}\boldsymbol{I_{\mathrm{R}}} + \left(\frac{1}{\mathrm{j}\omega C_{\mathrm{F}}} - \mathrm{j}\omega M_{\mathrm{T12}}\right)\boldsymbol{I_{\mathrm{T1}}} \\ 0 = \left(\mathrm{j}\omega L_{\mathrm{R}} + \frac{1}{\mathrm{j}\omega C_{\mathrm{R}}} + R_{\mathrm{EQ}}\right)\boldsymbol{I_{\mathrm{R}}} \\ +\mathrm{j}\omega M_{\mathrm{T1R}}\boldsymbol{I_{\mathrm{T1}}} - \mathrm{j}\omega M_{\mathrm{T2R}}\boldsymbol{I_{\mathrm{T2}}} \end{cases} \tag{11}$$

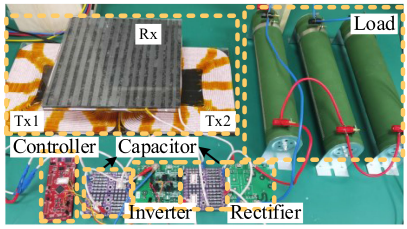

Fig. 8. Photograph of experimental prototype.

TABLE I
PARAMETERS OF EXPERIMENTAL PROTOTYPE

V_{INV}	300 V	f	85 kHz	R_{L}	30 Ω
C_{T1}, C_{T2}	22.61 nF	C_{F}	91.82 nF	C_{R}	18.28 nF
L_{T1}	194 μH	L_{T2}	194 μH	L_{R}	193 μH

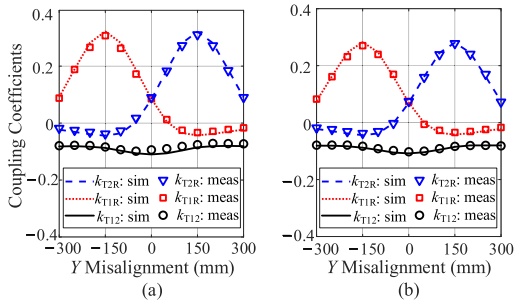

Fig. 9. Simulated and measured coupling coefficients. (a) $X = 0$. (b) $X = 50$ mm.

Combining (1) and (11), the input impedance Z_{IN} is

$$Z_{\mathrm{IN}} = \frac{X_{\mathrm{T}}(R_{\mathrm{EQ}}X_{\mathrm{T}} - \mathrm{j}2\omega M_{\mathrm{T1R}}\omega M_{\mathrm{T2R}})}{(\omega M_{\mathrm{T2R}})^2} \tag{12}$$

From Fig. 2, we can see that k_{T1R} and k_{T2R} (M_{T1R} and M_{T2R}) are of opposite signs, namely one is positive, and the other is negative. Therefore, Z_{IN} is inductive, able to achieve ZVS.

In this case when Tx2 acts as the power transmission coil, the output voltage, output power, and coil-to-coil efficiency are

$$V_{\mathrm{REC}} = \frac{V_{\mathrm{INV}}}{\sqrt{\frac{\pi^4}{4}\frac{(\omega M_{\mathrm{T1R}})^2}{R_{\mathrm{L}}^2} + \frac{4X_{\mathrm{T}}^2}{(\omega M_{\mathrm{T2R}})^2}}} \tag{13}$$

$$P_{\mathrm{OUT}} = \frac{V_{\mathrm{INV}}^2}{\frac{\pi^4}{4}\frac{(\omega M_{\mathrm{T1R}})^2}{R_{\mathrm{L}}} + \frac{4R_{\mathrm{L}}X_{\mathrm{T}}^2}{(\omega M_{\mathrm{T2R}})^2}} \tag{14}$$

$$\eta = \frac{P_{\mathrm{out}}}{P_{\mathrm{out}} + R_{\mathrm{T1}}I_{\mathrm{T1}}^2 + R_{\mathrm{T2}}I_{\mathrm{T2}}^2 + R_{\mathrm{R}}I_{\mathrm{R}}^2}. \tag{15}$$

Due to symmetry, with Tx1 as the power transmission coil, the expressions can be obtained by switching M_{T1R} and M_{T2R}. The use of the LCCC-S topology is to enhance the power transfer capability at the boundary positions (Regions II.1 and II.2).

When Rx locates at the central positions (Region I), the system is reconfigured to the S-S topology; at the boundary positions (Regions II.1 and II.2), the system is reconfigured to the LCCC-S topology. In this way, the high-efficiency stable output can be achieved.

IV. Experimental Validation

Based on the proposed WPT system, a prototype is built as shown in Fig. 8. The parameters of the prototype are tabulated in Table I. The initial point is defined as given in Fig. 1. Two X

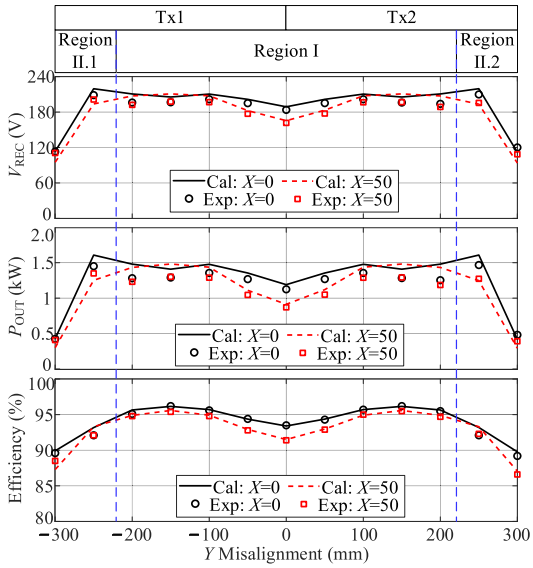

Fig. 10. Experimental results of output voltage, output power, and dc–dc efficiency with misalignments.

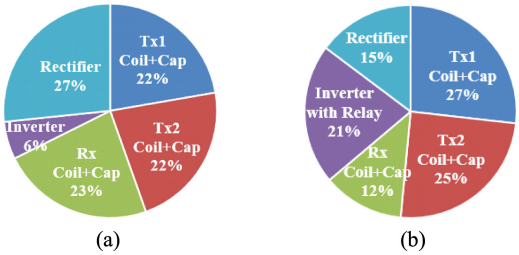

Fig. 11. Loss breakdown. (a) Mode I when $X = 0$ and $Y = 100$ mm. (b) Mode II when $X = 50$ mm and $Y = 250$ mm.

misalignment cases are studied, namely $X = 0$ and $X = 50$ mm. Y changes from -300 mm to 300 mm. The simulated and measured coupling coefficients are given in Fig. 9. The measured results match well with the simulations.

The experimental results of the output voltage, the output power, and the dc–dc efficiency varying with the Y misalignment under two X misalignment cases are shown in Fig. 10. A total tolerance of 500 mm Y misalignment and 100 mm X misalignment can be realized with stable output and high efficiency by using the proposed method.

The loss breakdown of two cases is depicted in Fig. 11. The experimental waveforms are depicted in Fig. 12.

V. Conclusion

This letter has proposed a misalignment-tolerant dual-transmitter EV wireless charging system with reconfigurable topologies. At central positions, the two transmitting coils can be connected in series to form the S-S topology. At boundary positions, the two transmitting coils can be reconfigured to form the LCCC-S topology, with one transmitting coil as the power transmission coil and the other as the compensating inductor. In this way, not only the output power can be smoothed with high efficiency, but also wireless charging is guaranteed at weak couplings. A total tolerance of 500 mm door-to-door misalignment and 100 mm front-rear misalignment can be realized with stable output and high efficiency by using the proposed method.

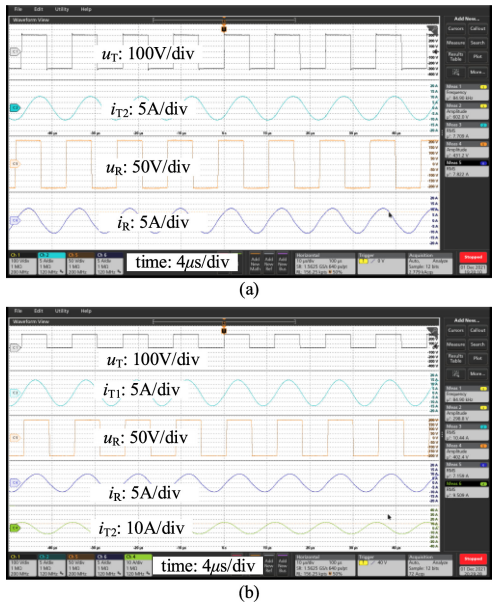

Fig. 12. Experimental waveforms. (a) Mode I when $X = 0$ and $Y = 100$ mm. (b) Mode II when $X = 50$ mm and $Y = 250$ mm.

References

[1] A. Ahmad, M. S. Alam, and R. Chabaan, "A comprehensive review of wireless charging technologies for electric vehicles," *IEEE Trans. Transport. Electrific.*, vol. 4, no. 1, pp. 38–63, Mar. 2018.

[2] Y. Zhang, S. Chen, X. Li, and T. Yi, "Design of high-power static wireless power transfer via magnetic induction: An overview," *CPSS Trans. Power Electron. Appl.*, vol. 6, no. 4, pp. 281–297, Dec. 2021.

[3] Y. Li *et al.*, "Extension of ZVS region of series–series WPT systems by an auxiliary variable inductor for improving efficiency," *IEEE Trans. Power Electron.*, vol. 36, no. 7, pp. 7513–7525, Jul. 2021.

[4] Y. Zhang, S. Chen, X. Li, Z. She, F. Zhang, and Y. Tang, "Coil comparison and downscaling principles of inductive wireless power transfer systems," in *Proc. IEEE PELS WoW*, 2020, pp. 116–122.

[5] K. Song *et al.*, "Design of DD coil with high misalignment tolerance and low EMF emissions for wireless electric vehicle charging systems," *IEEE Trans. Power Electron.*, vol. 35, no. 9, pp. 9034–9045, Sep. 2020.

[6] J. Mai, Y. Wang, Y. Yao, M. Sun, and D. Xu, "High-misalignment -tolerant IPT systems with solenoid and double d pads," *IEEE Trans. Ind. Electron.*, vol. 69, no. 4, pp. 3527–3535, Apr. 2022.

[7] Y. Zhang, S. Chen, X. Li, and Y. Tang, "Design methodology of free-positioning nonoverlapping wireless charging for consumer electronics based on antiparallel windings," *IEEE Trans. Ind. Electron.*, vol. 69, no. 1, pp. 825–834, Jan. 2022.

[8] W. S. Lee, W. I. Son, K. S. Oh, and J. W. Yu, "Contactless energy transfer systems using antiparallel resonant loops," *IEEE Tran. Ind. Electron.*, vol. 60, no. 1, pp. 350–359, Jan. 2013.

[9] W. Zhao, X. Qu, J. Lian, and C. K. Tse, "A family of hybrid IPT couplers with high tolerance to pad misalignment," *IEEE Trans. Power Electron.*, vol. 37, no. 3, pp. 3617–3625, Mar. 2022.

[10] Y. Chen *et al.*, "A hybrid inductive power transfer system with misalignment tolerance using Quadruple-D quadrature pads," *IEEE Trans. Power Electron.*, vol. 35, no. 6, pp. 6039–6049, Jun. 2020.

[11] L. Zhao, D. J. Thrimawithana, and U. K. Madawala, "Hybrid bidirectional wireless EV charging system tolerant to pad misalignment," *IEEE Trans. Ind. Electron.*, vol. 64, no. 9, pp. 7079–7086, Sep. 2017.

[12] C. Xia, W. Wang, S. Ren, X. Wu, and Y. Sun, "Robust control for inductively coupled power transfer systems with coil misalignment," *IEEE Trans. Power Electron.*, vol. 33, no. 9, pp. 8110–8122, Sep. 2018.

[13] T. Lee, S. Huang, S. Dai, and J. Su, "Design of misalignment-insensitive inductive power transfer via interoperable coil module and dynamic power control," *IEEE Trans. Power Electron.*, vol. 35, no. 9, pp. 9024–9033, Sep. 2020.

[14] F. P. Wijaya, T. Shimotsu, T. Saito, and K. Kondo, "A simple active power control for a high-power wireless power transmission system considering coil misalignment and its design method," *IEEE Trans. Power Electron.*, vol. 33, no. 11, pp. 9989–10002, Nov. 2018.